MODELLING AND SIMULATION OF THREE-PHASE FOUR-SWITCH VOLTAGE SOURCE INVERTER WITH SPACE VECTOR MODULATION

PHAM CONG DUY
Faculty of Electrical Engineering Technology, Industrial University of Ho Chi Minh City
dph@iuh.edu.vn
DOIs: https://doi.org/10.46242/jstiuh.v60i06.4633

Abstract. The three-phase six-switches voltage source inverter is usually used for industrial motor control and renewable energy systems. However, in order to decrease to size and cost of the drive systems, the three-phase four-switch voltage source inverter has been applied to low-cost motor control and renewable energy system. The fundamental concepts and principles of the three-phase four-switch voltage source inverter are discussed. The mathematical model and space vector modulation of the three-phase four-switch voltage source inverter are proposed. The work is demonstrated by simulation results.
Keywords. Three-phase four-switch voltage source inverter, space vector modulation, modelling and simulation, low-cost motor control, low-cost variable frequency drive.

1. INTRODUCTION

The key function of a three-phase six-switches voltage source inverter (SSTPI) is to transform a fixed DC voltage to a three-phase AC voltage with variable magnitude and frequency [1] which is consisted of six switches, $S_1 - S_6$, as given in Figure 1a. This inverter type has been used for industrial applications, including motor drives [2], wind power systems [3,4], and solar systems [5,6]. However, in practical applications, reducing inverter size and cost must be considered. To achieve this goal, three-phase inverter with only four switches has also been reported by [7] and it was named three-phase four-switches voltage source inverter (FSTPI). Normally, these power semiconductor switches devices can be IGBT and MOSFET, as seen in Figure 1b. Specially, the midpoint of the dc-link capacitors should be connected to only one phase of motor stator windings [8].
Recently, the FSTPIs have been proposed for low-cost brushless DC motor drive applications in [9-11]. In [9], a current control scheme of brushless DC motors driven by four-switch three-phase inverters was proposed. The direct torque control method of brushless DC motors to reduce torque ripple during sector-to-sector commutations has been shown in [10]. There has been a significant research interest to control of induction motors [12-15]. In [12], a performance investigation of FSTPI-fed induction motor drives at low speeds using fuzzy logic and PI controllers has been shown. The direct torque control method [13], the predictive torque control [14], and the finite-control-set model predictive control [15] for FSTPI-fed induction motor drives have been studied.
This inverter has been utilized in control to PMSM drives [16-18]. The influence and compensation of inverter voltage drop in direct torque control [16], predictive current control [17], and high-frequency voltage injection sensorless control for the FSTPI-fed permanent magnet synchronous motor drives. The other approach for this inverter was reported in [19] with synchronous reluctance motors drive systems.
This inverter has been intensively investigated to wind power [20-23]. In [20,21], the direct torque and power control techniques for fault-tolerant back-to-back converter for direct-drive PMSG wind turbines was considered. The two FSTPIs are connected to get a low-cost back-to-back converter for PMSG wind turbines using the hysteresis current controllers which was proposed in [22]. Application of the FSTPIs to connect renewable energy source to a generalized unbalanced microgrid system was shown in [23].
Correspondingly, various pulse width modulation (PWM) techniques for FSTPIs have been proposed in the literature [1]. With the research and development of digital signal processors, microcontrollers, and microprocessors, the space-vector modulation, a technique that get to less harmonic distortion of the load current and low switching losses that will not be required to use the add hardware devices. This technique uses a concept of a space vector, and it was named space vector pulse width modulation (SVPWM) [1].
For developing low-cost energy-saving products, the mathematical model and space vector modulation of the three-phase four-switch voltage source inverter technology are proposed in the paper. The paper will be

focused on both the undergraduate and postgraduate students of electrical engineering and automation control engineering at the Industrial University of Ho Chi Minh City, Vietnam.

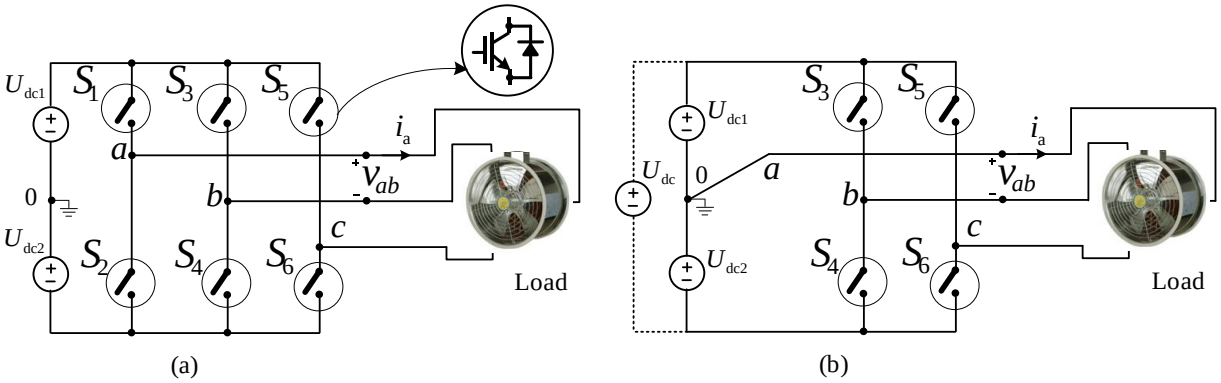

Figure 1: Circuit diagrams of the inverter-fed three-phase load. (a) SSTPI and (b) FSTPI.

Figure 1 shows the circuit diagrams of the inverter-fed three-phase load. Figure 1a shows the circuit diagram of the SSTPI and Figure 1b shows the circuit diagram of the FSTPI.
In this paper, the mathematical model, SVM, and the flowchart of the SVM algorithm implementation of three-phase four-switch inverter are proposed.
The main parts of the paper are briefly given as follows: Section 1 gives an introduction of SSTPIs and FSTPIs. Then, Section 2 recalls the model of the FSTPI. Section 3 proposes the flowchart of the SVM algorithm implementation. Numerical results are given in Section 4. Section 5 summarizes the conclusion of the paper.

2. MODEL OF THREE-PHASE FOUR-SWITCH VOLTAGE SOURCE INVERTER

In this section, the model of FSTPI is shown in Fig. 1b.
For simplicity, the switching states for each phase are the switching states (either off or on) which can be obtained as follows:

$$\begin{cases} S_b = S_3 \\ S_c = S_5 \end{cases} \tag{1}$$

The pole voltages of FSTPI can be calculated based on the switching states and the dc-link two-capacitor voltages U_{dc1} and U_{dc2}

$$\begin{cases} u_{ao} = 0 \\ u_{bo} = S_b U_{\text{dc1}} + (S_b - 1)U_{\text{dc2}} \\ u_{co} = S_c U_{\text{dc1}} + (S_c - 1)U_{\text{dc2}} \end{cases} \tag{2}$$

Under the assumption of three-phase balanced operation conditions, the phase-to-neutral voltages are listed as follows [16]

$$\begin{cases} u_{an} = \dfrac{2}{3}u_{ao} - \dfrac{1}{3}(u_{bo} + u_{co}) \\ u_{bn} = \dfrac{2}{3}u_{bo} - \dfrac{1}{3}(u_{co} + u_{ao}) \\ u_{cn} = \dfrac{2}{3}u_{co} - \dfrac{1}{3}(u_{ao} + u_{bo}) \end{cases} \tag{3}$$

From Figure 1b, with combination of the S_b and S_c switches, there are four switching status of S_b and S_c switches, such as, (off, off), (off, on), (on, off), and (on, on) which are shown in Figure 2a, Figure 2b, Figure 2c, and Figure 2d, respectively.

Applying to Kirchhoff's voltage law of Figure 2, the sector number, switching states, and the output voltages of the FSTPI are listed in Table 1.

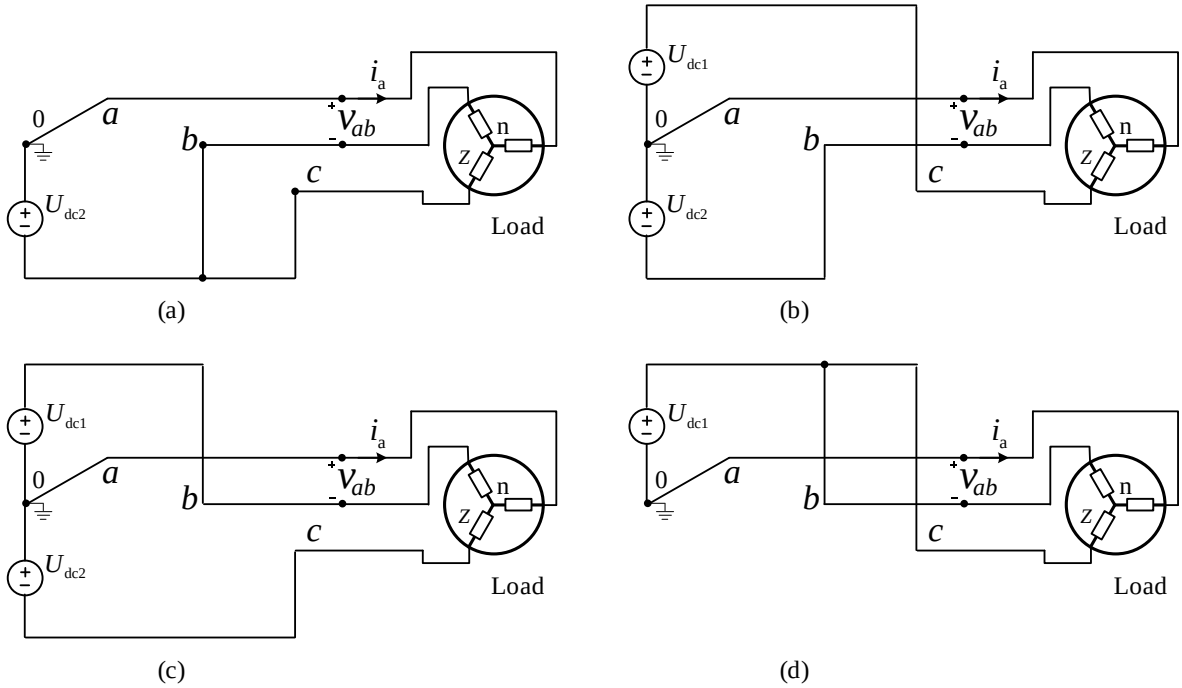

Figure 2: The four switching states. (a) $S_b = \text{off}, S_c = \text{off}$, (b) $S_b = \text{off}, S_c = \text{on}$, (c) $S_b = \text{on}, S_c = \text{off}$, (d) $S_b = \text{on}, S_c = \text{on}$

Table 1: Switching state and the output voltages of the FSTPI

Sector number	Sector volatge	Switching state (S_b, S_c)	Ouput volatge u_{an}	Ouput volatge u_{bn}	Ouput volatge u_{cn}
1	U_1	off, off	$\frac{2}{3}U_{dc2}$	$-\frac{1}{3}U_{dc2}$	$-\frac{1}{3}U_{dc2}$
2	U_2	off, on	$\frac{1}{3}(U_{dc2}-U_{dc1})$	$-\frac{1}{3}(2U_{dc2}+U_{dc1})$	$\frac{1}{3}(2U_{dc1}+U_{dc2})$
3	U_3	on, off	$\frac{1}{3}(U_{dc2}-U_{dc1})$	$\frac{1}{3}(2U_{dc1}+U_{dc2})$	$-\frac{1}{3}(2U_{dc2}+U_{dc1})$
4	U_4	on, on	$-\frac{2}{3}U_{dc1}$	$\frac{1}{3}U_{dc1}$	$\frac{1}{3}U_{dc1}$

Based on Table 1, the phase-to-neutral voltages are functions of the S_b and S_c switches and the dc-link two-capacitor voltages U_{dc1} and U_{dc2}, then there is

$$\begin{cases} u_{an} = \dfrac{U_{dc1}}{3}(-S_b - S_c) + \dfrac{U_{dc2}}{3}(2 - S_b - S_c) \\ u_{bn} = \dfrac{U_{dc1}}{3}(2S_b - S_c) + \dfrac{U_{dc2}}{3}(2S_b - S_c - 1) \\ u_{cn} = \dfrac{U_{dc1}}{3}(2S_c - S_b) + \dfrac{U_{dc2}}{3}(2S_c - S_b - 1) \end{cases} \quad (4)$$

Considering the dc-link voltage value of upper capacitance and the dc-link voltage value of lower capacitance are equal, given by

$$U_{\text{dc1}} = U_{\text{dc2}} = \frac{U_{\text{dc}}}{2} \tag{5}$$

Substituting (5) into (4), we have

$$\begin{cases} u_{an} = \dfrac{U_{\text{dc}}}{6}(2 - 2S_b - 2S_c) \\ u_{bn} = \dfrac{U_{\text{dc}}}{6}(4S_b - 2S_c - 1) \\ u_{cn} = \dfrac{U_{\text{dc}}}{6}(4S_{\text{c}} - 2S_{\text{b}} - 1) \end{cases} \tag{6}$$

Equation (6) shows the mathematical model of the three-phase four-switch voltage source inverter.

3. SPACE VECTOR MODULATION

This section presents the theory and implementation of the space vector modulation for the FSTPI. The main task of the SVPWM is to determine the switching signals for the FSTPI, then generating the three-phase voltages with variable magnitude and frequency to the three-phase loads. By combining the switching states and the space vectors, the reference voltage vector v_{ref} was created instantaneously.

The three-phase control voltages are given by [24,25]

$$\begin{cases} v_{\text{as}}^{*} = \sqrt{2}V\cos(2\pi ft) \\ v_{\text{bs}}^{*} = \sqrt{2}V\cos(2\pi ft - \dfrac{2\pi}{3}) \\ v_{\text{cs}}^{*} = \sqrt{2}V\cos(2\pi ft - \dfrac{4\pi}{3}) \end{cases} \tag{7}$$

in which V is the rms value of the control phase voltages and f is the frequency of the control phase voltages

To implement the SVPWM, three-phase abc reference voltages are converted into the alpha-beta reference voltages using the Clark transformation. Therefore, there is

$$\begin{cases} v_{\alpha\text{s}}^{*} = v_{\text{as}}^{*} \\ v_{\beta\text{s}}^{*} = \dfrac{2}{\sqrt{3}}(v_{\text{bs}}^{*} - v_{\text{cs}}^{*}) \end{cases} \tag{8}$$

Next, the magnitude and angular of the reference voltage vector are calculated from the alpha-beta reference voltages which may be rewritten as

$$\begin{cases} v_{\text{sref}}^{*} = U_s = \sqrt{(v_{\alpha\text{s}}^{*})^2 + (v_{\beta\text{s}}^{*})^2} \\ \theta = \tan^{-1}\dfrac{v_{\beta\text{s}}^{*}}{v_{\alpha\text{s}}^{*}} \end{cases} \tag{9}$$

The modified angular θ_n are calculated from the θ angular, then there is

$$\theta_n = \frac{180}{\pi}\theta \tag{10}$$

The sector number are calculated from the modified angular θ_n

$$\mathrm{n}=\begin{cases}1,\ (\theta_n>0^0 \text{ and } \theta_n\le 90^0)\\ 2,\ (\theta_n>90^0 \text{ and } \theta_n\le 180^0)\\ 3,\ (\theta_n\ge -180^0 \text{ and } \theta_n\le -90^0)\\ 4,\ (\theta_n\ge -90^0 \text{ and } \theta_n\le 0^0)\end{cases} \tag{11}$$

The modulation index can be calculated by

$$m_{\mathrm{a}}=\frac{\sqrt{3}U_{\mathrm{s}}}{U_{\mathrm{dc}}} \tag{12}$$

The reference voltage vector is synthesized using vectors U_1 to U_4

$$\int_0^{T_{\mathrm{s}}} U_s dt=\int_0^{T_{00}} U_1 dt+\int_{T_{00}}^{T_{00}+T_{10}} U_2 dt+\int_{T_{00}+T_{10}}^{T_{00}+T_{10}+T_{11}} U_3 dt+\int_{T_{00}+T_{10}+T_{11}}^{T_{00}+T_{10}+T_{11}+T_{01}} U_4 dt \tag{13}$$

The dwell times for the vectors U_1 to U_4

$$\begin{cases}U_s T_{\mathrm{s}}=U_1T_{00}+U_2T_{10}+U_3T_{11}+U_4T_{01}\\ T_{\mathrm{s}}=T_{00}+T_{10}+T_{11}+T_{01}\end{cases} \tag{14}$$

The duty ratios can be calculated by

$$\begin{cases}T_{\mathrm{b}}=\frac{T_{\mathrm{s}}}{2}(-T_{00}+T_{10}+T_{11}-T_{01})\\ T_{\mathrm{c}}=\frac{T_{\mathrm{s}}}{2}(-T_{00}-T_{10}+T_{11}+T_{01})\end{cases} \tag{15}$$

Finally, the duty ratios T_{b} and T_{c} are comparing with the carrier wave tri to the switches S_b and S_c [24,25].

$$\begin{cases}S_b=T_{\mathrm{b}}\ge tri\\ S_c=T_{\mathrm{c}}\ge tri\end{cases} \tag{16}$$

Table 2: The sector and the dwell times of the FSTPI

Sector I	Sector II
$T_{00}=\frac{T_{\mathrm{s}}}{2}-m_{\mathrm{a}}T_{\mathrm{s}}\sin(\theta-\frac{\pi}{3})$ $T_{01}=0$ $T_{10}=m_{\mathrm{a}}T_{\mathrm{s}}\sin(\theta)$ $T_{11}=\frac{T_{\mathrm{s}}}{2}-m_{\mathrm{a}}T_{\mathrm{s}}\sin(\theta+\frac{\pi}{3})$	$T_{00}=0$ $T_{01}=\frac{T_{\mathrm{s}}}{2}-m_{\mathrm{a}}T_{\mathrm{s}}\sin(\theta-\frac{\pi}{3})$ $T_{10}=\frac{T_{\mathrm{s}}}{2}-m_{\mathrm{a}}T_{\mathrm{s}}\sin(\theta+\frac{\pi}{3})$ $T_{11}=-\sqrt{3}m_{\mathrm{a}}T_{\mathrm{s}}\sin(\theta)$
Sector III	**Sector IV**
$T_{00}=\frac{T_{\mathrm{s}}}{2}+m_{\mathrm{a}}T_{\mathrm{s}}\sin(\theta+\frac{\pi}{3})$ $T_{01}=-m_{\mathrm{a}}T_{\mathrm{s}}\sin(\theta)$ $T_{10}=0$ $T_{11}=\frac{T_{\mathrm{s}}}{2}+m_{\mathrm{a}}T_{\mathrm{s}}\sin(\theta-\frac{\pi}{3})$	$T_{00}=\sqrt{3}m_{\mathrm{a}}T_{\mathrm{s}}\sin(\theta)$ $T_{01}=\frac{T_{\mathrm{s}}}{2}-m_{\mathrm{a}}T_{\mathrm{s}}\sin(\theta+\frac{\pi}{3})$ $T_{10}=\frac{T_{\mathrm{s}}}{2}+m_{\mathrm{a}}T_{\mathrm{s}}\sin(\theta-\frac{\pi}{3})$ $T_{11}=0$

Based on (14), we have Table 2. There are six main steps for the implementation process of the SVM.

First, according to (7), the control phase voltages v_{as}^{*}, v_{bs}^{*}, and v_{cs}^{*} are the initial conditions of the step 1.

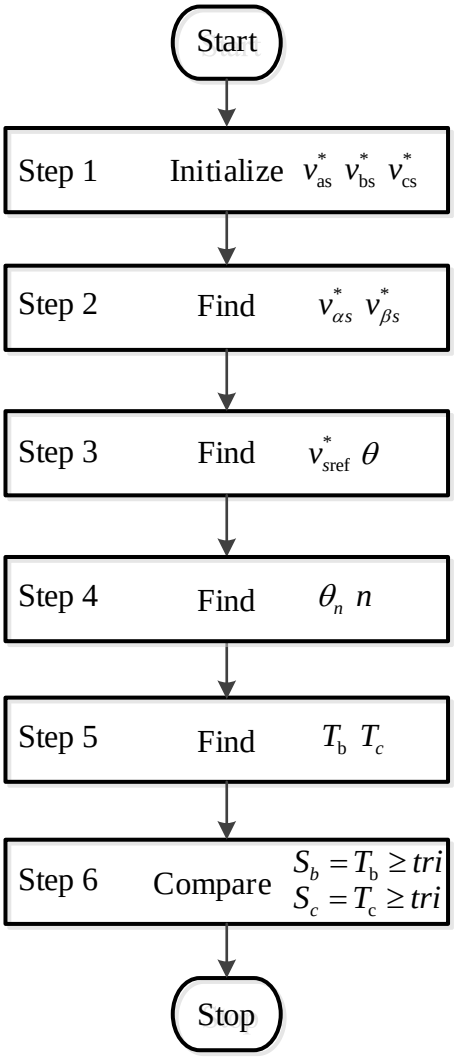

Figure 3: Flowchart of the SVM algorithm implementation

Then, the step 2 uses the Clark transformation to find the control phase voltages $v_{\alpha s}^{*}$ and $v_{\beta s}^{*}$. The step 3 is implemented to find the v_{ref}^{*} and $\theta^{'}$. Finally, the switching signals for the FSTPI are generated by comparing duty ratios T_b and T_c to the carrier wave tri. Figure 3 shows the flowchart of the implementation of space vector modulation of the three-phase four-switch voltage source inverter.

4. SIMULATION RESULTS AND DISCUSSION

By demonstrating the performance of SVM mentioned above, a program is developed in Matlab/Simulink environment. The parameters of the simulation system are listed in Table 3 and Table 4. The dc-link voltage is 550 V, amplitude value of phase voltages is 220 V, control frequency is 50 Hz, switching frequency is 4 kHz.

The simulated waveforms for the SVM are shown in Figure 4. Figure 4a shows how the phase voltages of the control waveform is obtained which are equal to those of the three-phase reference voltage having the rms value of phase voltages is 220 V and the frequency is 50 Hz . Figure 4b shows the alpha-beta reference voltages and they also have the rms value of phase voltages is 220 V and the frequency is 50 Hz. Figure 4c shows the magnitude of the reference voltage which is 230 V. Figure 4d shows the angular of the reference

voltage. Figure 4e shows sector number from 4 to 1. These results are the same as Equation 11. It can be observed from Figure 4f that the modulation index is 0.73. Figure 4g shows the duty ratios for the switches S_b and S_c. Figure 4h shows the gate signal of the switches S_b and S_c. It can be shown that the gate signal of the switch S_b and the gate signal of the switch S_c are opposite each other.

Figure 5 shows the performance of three-phase load including the load voltages and the load currents. Figure 5a shows the load voltage of the *a*-phase. Figure 5b shows the load voltage of the *b*-phase. Figure 5c shows the load voltage of the *c*-phase. Figure 5d shows the three-phase load currents which is close to sinusoidal waveform and the magnitude value of them are about 2 A.

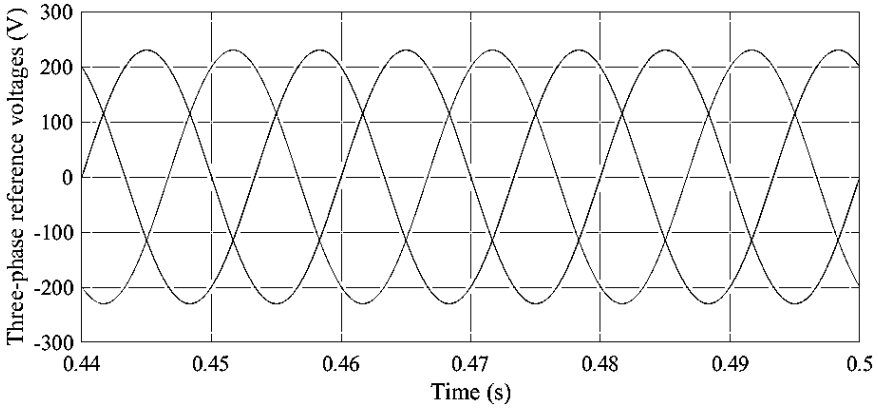

(a)

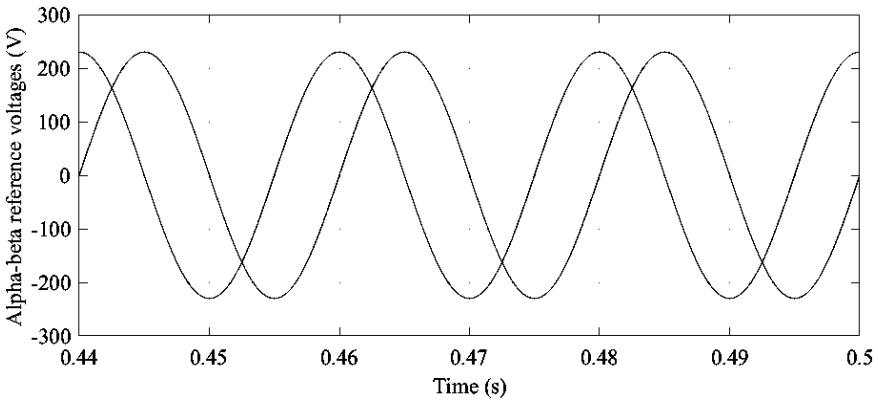

(b)

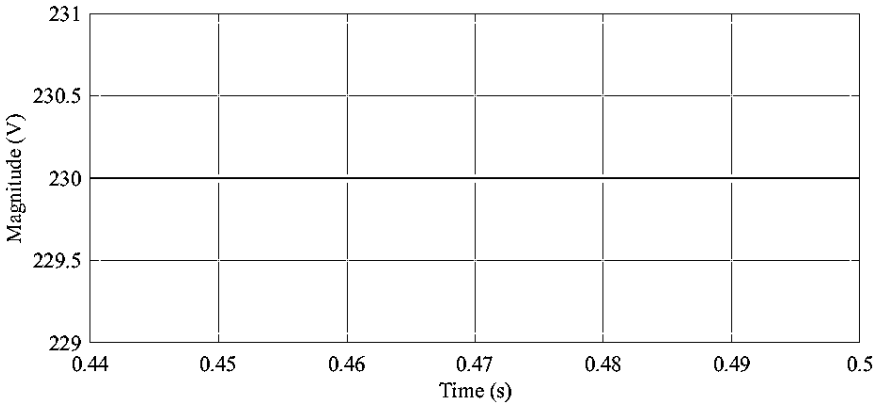

(c)

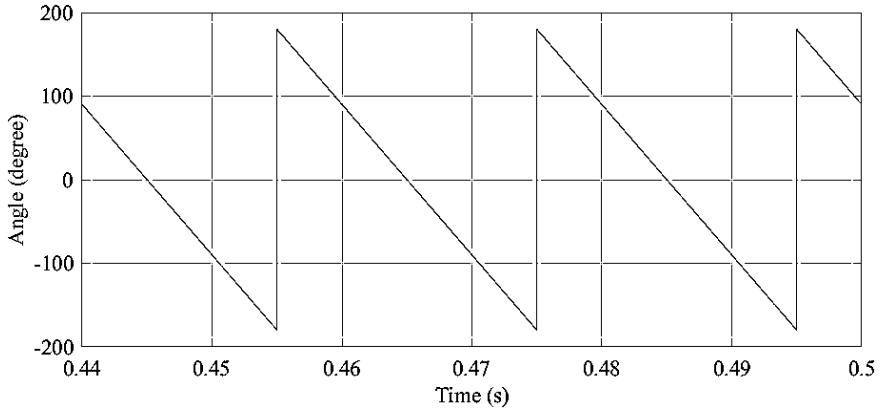
200
100
0
-100
-200
Angle (degree)
0.44
0.45
0.46
0.47
0.48
0.49
0.5
Time (s)

(d)

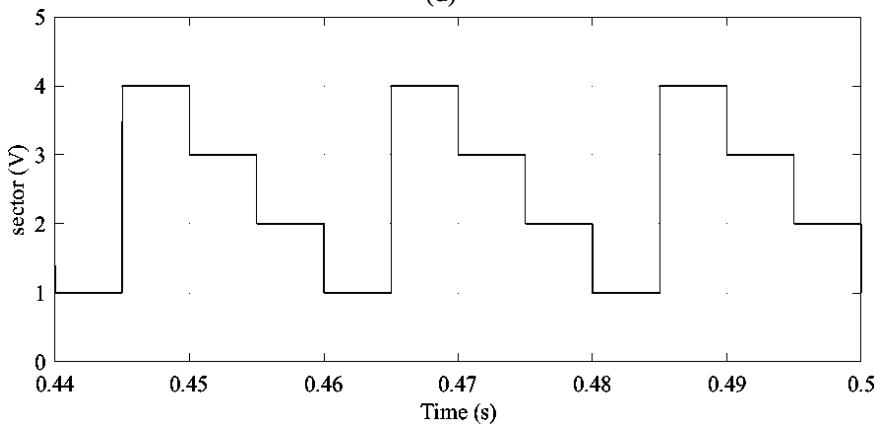
5
4
3
2
1
0
sector (V)
0.44
0.45
0.46
0.47
0.48
0.49
0.5
Time (s)

(e)

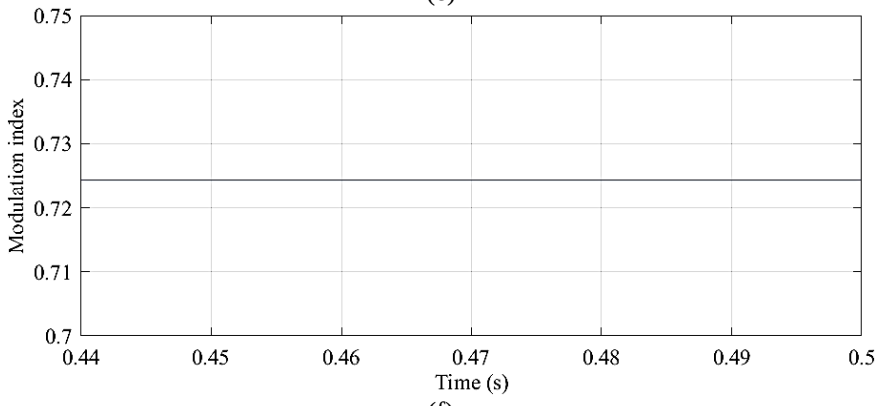
0.75
0.74
0.73
0.72
0.71
0.7
Modulation index
0.44
0.45
0.46
0.47
0.48
0.49
0.5
Time (s)

(f)

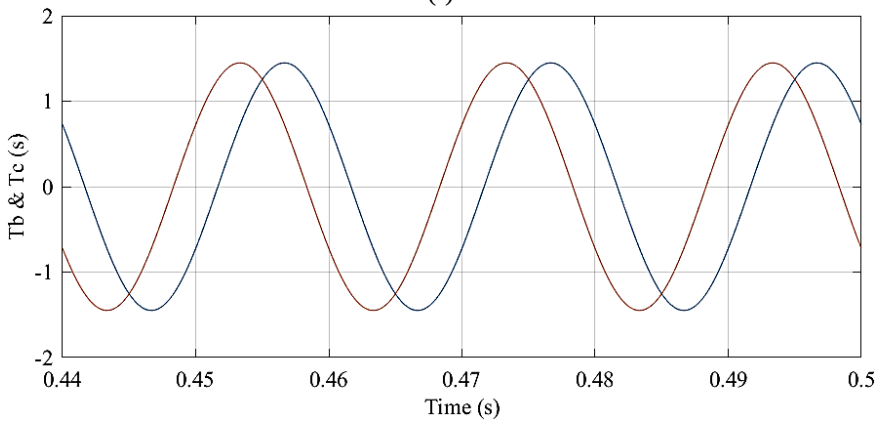
2
1
0
-1
-2
Tb & Tc (s)
0.44
0.45
0.46
0.47
0.48
0.49
0.5
Time (s)

(g)

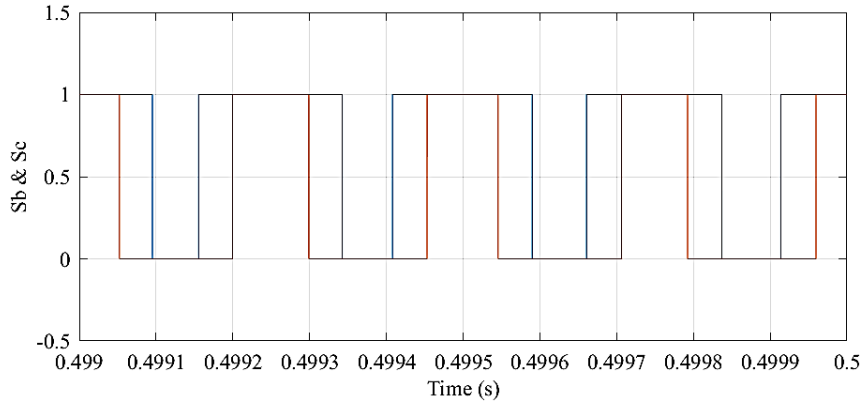

(h)

Figure 4: SVM inverter. (a) phase voltages of the control, (b) the alpha-beta reference voltages, (c) the magnitude of the reference voltage, (d) the angular of the reference voltage, (e) sector number, (f) the modulation index, (g) the duty ratios, (h) the gate signals.

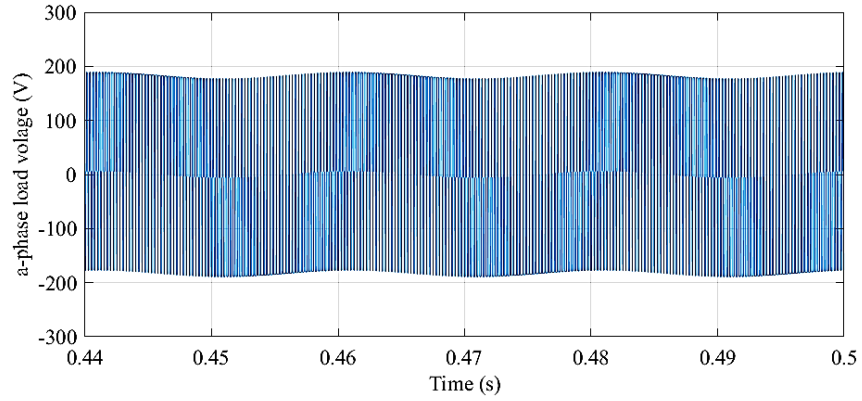

(a)

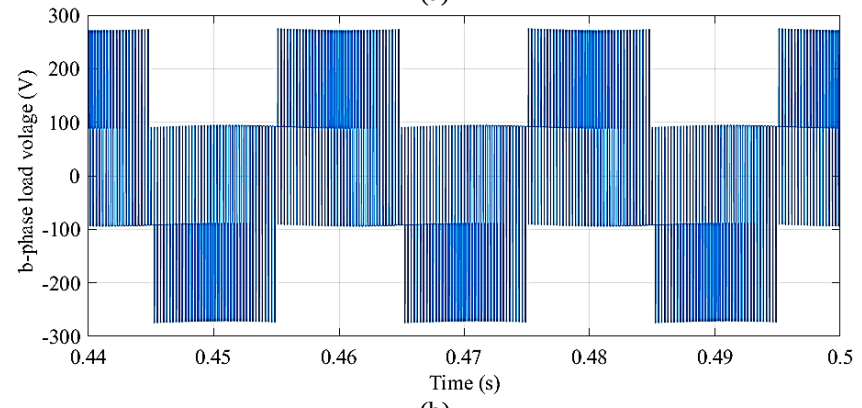

(b)

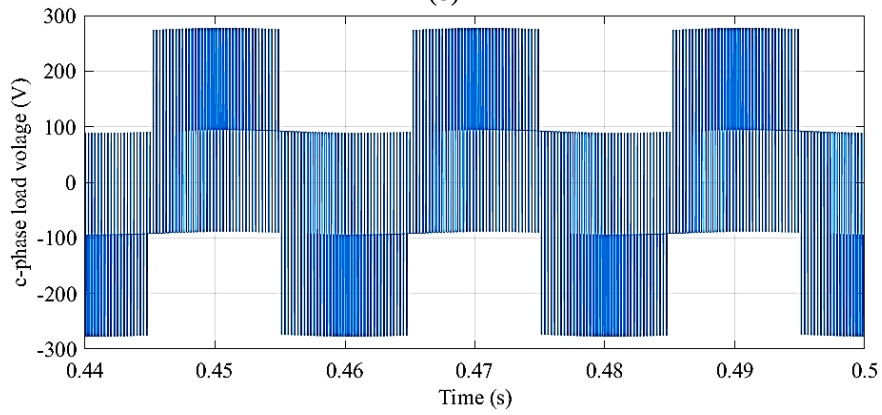

(c)

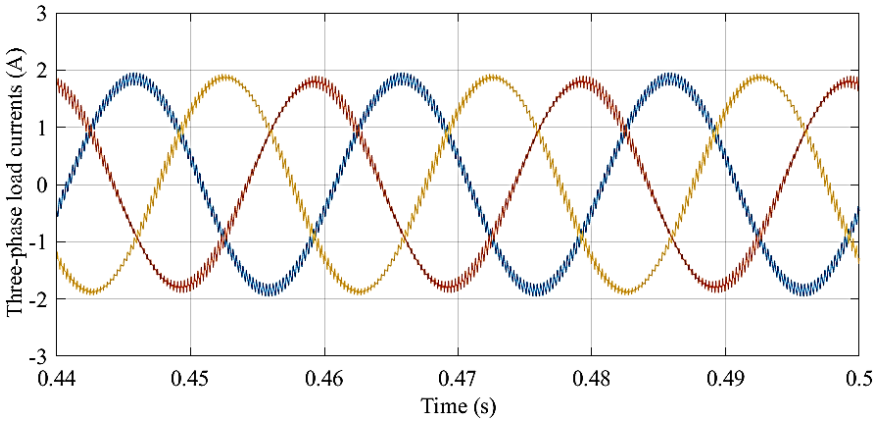

(d)

Figure 5: Performance of three-phase load. (a) the load voltage of the *a*-phase, (b) the load voltage of the *b*-phase, (c) the load voltage of the *c*-phase, (d) the three-phase load currents.

Table 3: IGBT parameters

Symbol	Value	Descriptions
R_{on}	0.001 Ω	Internal resistance
R_s	100 kΩ	Snubber resistance
C_s	inf	Snubber capacitive

Table 4: Load parameters

Symbol	Value	Descriptions
R	60 Ω	Load resistance
L	0.06 H	Load inductance

5. CONCLUSIONS

This paper has presented the SVPWM for FSTP. The simulation results demonstrate the proposed approach. The approach can easily be implemented in low-cost reduced switch inverters. This paper is also a reference for the students in the field of electrical machines control. In addition, this approach can also be extended for pump and fan solutions in high-tech agriculture applications.
Future works will been consider the processor-in-the-loop approach such as LAUNCHXL-F28069M for FSTPs to get reduction of the total harmonic distortion and common mode voltage in low-cost motor control and renewable energy systems.

REFERENCES

[1] B. Bose, *Power electronics and motor drives: Advances and Trends*, 2nd edition. United States: Academic Press, 2020.
[2] X. Yang, G. Liu, V. D. Le, and C. Q. Le, "A novel model- predictive direct control for induction motor drives", *IEEJ Trans. Electrical and Electronic Engineering*, vol. 14, no. 11, pp. 1691-1702, 2019. DOI: 10.1002/tee.22992.
[3] B. Wu, Y. Lang, N. Zargari, and S. Kouro, *Power conversion and control of wind energy systems.* United States: Wiley-IEEE Press, 2011.
[4] X. Yang, G. Liu, A. Li, and L. V. Dai, "A predictive power control strategy for DFIGs based on a wind energy converter system", *Energies*, vol. 10, no. 8, pages 1098, 2017. DOI: 10.3390/en10081098.
[5] W. Xiao, *Photovoltaic Power System: Modeling, Design, and Control*. United States: Wiley Press, 2017.

[6] T. T. Nguyen, T. D. Pham, L. C. Kien, and L. V. Dai, "Improved coyote optimization algorithm for optimally installing solar photovoltaic distribution generation units in radial distribution power systems", *Complexity*, 2020. DOI: 10.1155/2020/1603802.
[7] J. F. Khana, S. M.A. Bhuiyana, K. M. Rahmanb, and G. V. Murphya, "Space vector PWM for a two-phase VSI", *International Journal of Electrical Power & Energy Systems*, vol. 51, pp. 265-277, 2013. DOI:10.1016/j.ijepes.2013.02.029.
[8] R. Wang, J. Zhao, Y. Liu, "A comprehensive investigation of four-switch three-phase voltage source inverter based on double fourier integral analysis", *IEEE Trans. Power Electron.*, vol. 26, no. 10, 2011. DOI: 10.1109/TPEL.2011.2119381.
[9] C. Xia, D. Wu, T. Shi, and W. Chen, "A Current Control Scheme of Brushless DC Motors Driven by Four-Switch Three-Phase Inverters", *IEEE Journal of Emerging and Selected Topics in Power Electron*., vol. 5, no. 1, pp. 547 – 558, 2017. DOI: 10.1109/JESTPE.2016.2637383.
[10] M. Masmoudi, B. E. Badsi, and A. Masmoudi, "DTC of B4-Inverter-Fed BLDC Motor Drives With Reduced Torque Ripple During Sector-to-Sector Commutations", *IEEE Trans. Power Electron.*, vol. 29, no. 9, pp. 4855 – 4865, 2014. DOI: 10.1109/TPEL.2013.2284111.
[11] F. Naseri, E. Farjah, E. Schaltz, K Lu, and N. Tashakor, "Predictive Control of Low-Cost Three-Phase Four-Switch Inverter-Fed Drives for Brushless DC Motor Applications", *IEEE Trans. Circuits and Systems I: Regular Papers*, vol. 68, no. 3, pp. 1308 – 1318, 2021. DOI: 10.1109/TCSI.2020.3043468.
[12] M. S. Zaky and M. K. Metwaly, "A Performance Investigation of a Four-Switch Three-Phase Inverter-Fed IM Drives at Low Speeds Using Fuzzy Logic and PI Controllers", *IEEE Trans. Power Electron.*, vol. 32, no. 5, pp. 3741 – 3753, 2017. DOI: 10.1109/TPEL.2016.2583660.
[13] B. E. Badsi, B. Bouzidi, and A. Masmoudi, "DTC Scheme for a Four-Switch Inverter-Fed Induction Motor Emulating the Six-Switch Inverter Operation", *IEEE Trans. Power Electron.*, vol. 28, no. 7, pp. 3528 – 3538, Jul. 2013. DOI: 10.1109/TPEL.2012.2225449.
[14] D. Zhou, J. Zhao, and Y. Liu, "Predictive Torque Control Scheme for Three-Phase Four-Switch Inverter-Fed Induction Motor Drives With DC-Link Voltages Offset Suppression", *IEEE Trans. Power Electron.*, vol. 30, no. 6, pp. 3309 – 3318, 2015. DOI: 10.1109/TPEL.2014.2338395.
[15] D. Zhou, J. Zhao, and Y. Liu, "Finite-control-set model predictive control scheme of three-phase four-leg back-to-back converter-fed induction motor drive", *IET Electric Power Appl.*, vol. 11, no. 5, pp. 761-767, 2017. DOI: 10.1049/iet-epa.2015.0617
[16] K. D. Hoang, Z. Q. Zhu, and M. P. Foster, "Influence and Compensation of Inverter Voltage Drop in Direct Torque-Controlled Four-Switch Three-Phase PM Brushless AC Drives", *IEEE Trans. Power Electron.*, vol. 26, no. 8, pp. 2343 – 2357, 2011. DOI: 10.1109/TPEL.2010.2096561.
[17] C. A. Agustin, J. Yu, C. Lin, J. Jai, and Y. Lai, "Triple-Voltage-Vector Model-Free Predictive Current Control for Four-Switch Three-Phase Inverter-Fed SPMSM Based on Discrete-Space-Vector Modulation", *IEEE Access*, vol. 9, pp. 60352 – 60363, 2021. DOI: 10.1109/ACCESS.2021.3074067.
[18] J. Lu, Y. Hu, X. Zhang, Z. Wang, J. Liu, and C. Gan, "High-Frequency Voltage Injection Sensorless Control Technique for IPMSMs Fed by a Three-Phase Four-Switch Inverter With a Single Current Sensor", *IEEE/ASME Trans. Mechatron.*, vol. 23, no 2, pp. 758 – 768, Apr. 2018. DOI: 10.1109/TMECH.2018.2803772.
[19] C. Lin, C. A. Agustin, J. Yu, Y. Cheng, F. Chen, and Y. Lai, "A Modulated Model-Free Predictive Current Control for Four-Switch Three-Phase Inverter-Fed SynRM Drive Systems", *IEEE Access*, vol. 9, pp. 162984 – 162995, 2021. DOI: 10.1109/ACCESS.2021.3133023.
[20] I. Jlassi and A. J. M. Cardoso, "Fault-Tolerant Back-to-Back Converter for Direct-Drive PMSG Wind Turbines using Direct Torque and Power Control Techniques", *IEEE Trans. Power Electron.*, vol. 34, no. 11, pp. 11215 – 11227, 2019. DOI: 10.1109/TPEL.2019.2897541.
[21] N. M. A. Freire, and A. J. M Cardoso, "A Fault-Tolerant Direct Controlled PMSG Drive for Wind Energy Conversion Systems", *IEEE Trans. Ind. Electron.*, vol. 61, no. 2, pp. 821 – 834, 2014. DOI: 10.1109/TIE.2013.2251734.
[22] M. A. Soliman, H. M. Hasanien, A. Durra, and M. Debouza, "High performance frequency converter controlled variable-speed wind generator using linear-quadratic regulator controller", *IEEE Trans. Ind. Appl.*, vol. 56, no. 5, pp. 5489 – 5498, 2020. DOI: 10.1109/TIA.2020.2996956.
[23] S. Dasgupta, S. N. Mohan, S. K. Sahoo, and S. K. Panda, "Application of Four-Switch-Based Three-Phase Grid-Connected Inverter to Connect Renewable Energy Source to a Generalized Unbalanced Microgrid System", *IEEE Trans. Ind. Electron.*, vol. 60, no. 3, pp. 1204 – 1215, 2013. DOI: 10.1109/TIE.2012.2202350.
[24] A. Hughes and B. Drury, *Electric motors and drives: Fundamentals, Types, and Applications*, 4th edition. United States: Elsevier, 2013.
[25] K. Sundareswaran, *Elementary concepts of power electronic drives*. United States: CRC Press, 2019.

MÔ HÌNH VÀ MÔ PHỎNG BIẾN TẦN BA PHA BỐN KHÓA VỚI QUÁ ĐIỀU CHẾ VECTOR KHÔNG GIAN

PHẠM CÔNG DUY
Khoa Công nghệ Điện, Trường Đại học Công nghiệp Thành phố Hồ Chí Minh.
dph@iuh.edu.vn

Tóm tắt. Biến tần nguồn áp ba pha sáu khóa được sử dụng cho điều khiển động cơ công nghiệp và hệ thống năng lượng tái tạo. Tuy nhiên, để giảm kích thước và giá thành của hệ thống truyền động, biến tần nguồn áp ba pha bốn khóa đã được áp dụng để điều khiển động cơ công suất thấp và hệ thống năng lượng tái tạo công suất thấp. Các khái niệm và nguyên lý cơ bản của bộ biến tần ba pha bốn khóa được thảo luận. Mô hình toán học và phương pháp điều chế vector không gian áp dụng cho bộ biến tần này được đề xuất. Công việc được chứng minh bởi kết quả mô phỏng.

Từ khóa. Biến tần nguồn áp bốn khóa ba pha, quá điều chế vector không gian, mô hình và mô phỏng, điều khiển động cơ giá thấp, truyền động tần số thay đổi giá thấp.

Received on: 23/02/2022

Accepted on: 12/07/2022